Detection of land cover change in the Brazilian Cerrado using radar data (Sentinel-1A)

Thaise Rodrigues [1]
Edson Eyji Sano [2]
Tati de Almeida [3]
Joselisa Maria Chaves [4]
Juan Doblas [5]

Abstract
The detection of changes in the natural vegetation of the Cerrado (Brazilian tropical savanna) has been conducted based on optical satellite images. With the open availability of Sentinel-1A satellite radar images, continuous, near-real-time monitoring of land-use changes has become a reality. The objective of this study was to analyze the potential of Sentinel-1A satellite radar images to detect changes in the natural vegetation cover of the Cerrado for the purpose of law enforcement procedures to control illegal deforestation. The test site was western Bahia State, northeast Brazil. We selected two Sentinel-1A scenes obtained on October 3, 2016 (T0) and October 27, 2017 (T1) (C-band, 20-meter spatial resolution, VV and VH polarizations). A set of 159 deforestation polygons identified in the Landsat-8 Operational Land Imager (OLI) satellite images from 2016 and 2017 (eight scenes) were used as training samples to define the typical radar backscattering coefficients (σ°) from the areas corresponding to the changes in the natural vegetation cover. The potential of the change detection technique was analyzed based on the boxplots involving the σ° values derived from the ratio T1/T0 (both without filtering and processed by the refined Lee and Quegan & Yu filters). Three thresholds were considered for each polarization. All radar image processing was conducted on the Google Earth Engine platform. The best result was obtained for the combination of VH, refined Lee, and a threshold of 0.60, which presented 95% overall accuracy and a 39% omission error.
Keywords: Savanna. Western Bahia State. Remote sensing. Backscattering.

Introduction

The Cerrado (Brazilian tropical savanna) biome is the second largest biome in Brazil and occupies an area of approximately 2 million km² in the

[1] Universidade de Brasília, Brasília, DF, Brasil. thaisesrodrigues@gmail.com
[2] Embrapa Cerrados, Planaltina, DF, Brasil. edson.sano@embrapa.br
[3] Universidade de Brasília, Brasília, DF, Brasil. tati_almeida@unb.br
[4] Universidade Estadual de Feira de Santana, Feira de Santana, BA, Brasil. joselisa@uefs.br
[5] Instituto Nacional de Pesquisas Espaciais, São José dos Campos, SP, Brasil. juan.doblas@inpe.br

central part of the country (SILVA; BATES, 2002). Despite its rich biodiversity, only 8.2% of its territory is protected by law. Of this total, only 2.9% corresponds to fully protected areas (ecological stations, natural monuments, national parks, wildlife refuges, and biological reserves) (MMA, 2018).

Extensive areas of the Cerrado have already been converted to soybean, maize, cotton, coffee, and sugarcane plantations, with soybean cultivation being the most prominent (SANO et al., 2010; RADA, 2013; CARNEIRO FILHO; COSTA, 2016). From 2000 to 2014, the growth in area of the soybean plantations in the Cerrado was 253% (CARNEIRO FILHO; COSTA, 2016). In regions such as Matopiba (a continuous Cerrado area covering part of the states of Maranhão, Tocantins, Piauí, and Bahia in northern and northeastern Brazil), more than 60% of agricultural expansion occurred in areas of native vegetation during that period. In the Matopiba region, we highlight western Bahia, which has become one of the main frontiers of national grain production since the 1980s (BRANNSTROM et al., 2008; MENKE et al., 2009; FLORES et al., 2012). The Cerrado occupation process in western Bahia occurred at high speed, where several factors contributed to the advance of agricultural expansion, including government financial incentives, the gentle topography, favorable agricultural mechanization, and the availability of low-price lands (MONDARDO, 2010; SANTOS et al., 2010).

Within this context, there was a need for the development of operational systems to detect deforestation in the Cerrado, mainly to monitor and control illegal deforestation. The systems based on optical images are limited in regions with persistent cloud cover and in regions where there is difficulty of differentiating some phytophysiognomies because of high spectral mixture, which is the case for the Cerrado (FERREIRA et al., 2007). One alternative or a complement of the optical systems designed to monitor deforestation are systems based on radar data. The advantage of radar

sensors is their ability to obtain images regardless of cloud coverage and their independence in terms of the variations in solar illumination conditions (MENESES; ALMEIDA, 2012). On April 3, 2014, the European Space Agency (ESA) launched the Sentinel-1A radar satellite, which operates in the C-band (~5 cm wavelength), VV and VH polarizations (V = vertical polarization; H = horizontal polarization), and a spatial resolution of 20 meters in the Interferometric Wide (IW) imaging mode (TORRES et al., 2012; ESA, 2013). For the first time, Sentinel-1A radar data are being made available at no cost on the internet. To date, there have been no studies evaluating the potential of Sentinel-1A imaging to detect changes in the natural Cerrado vegetation. The aim of this study was to analyze the potential of the Sentinel-1A satellite radar images to detect changes in the natural vegetation cover of the Cerrado for the purpose of monitoring and controlling illegal deforestation.

Materials and Methods

The study area is located between 11º 26' 42" and 12º 43' 08" south latitude and between 46º 09' 43" and 44º 36' 11" west longitude, covering most of the municipality of Barreiras, and corresponds to the overlapping areas between the Sentinel-1 and Landsat-8 images considered in this study. The selected area covers a region of approximately 19 thousand km² and includes portions of the municipalities of Angical, Barreiras, Baianópolis, Cristópolis, Catolândia, Luís Eduardo Magalhães, Riachão das Neves, and São Desidério in the western portion of Bahia State (Northeast Brazil), and portions of the municipalities of Dianópolis, Novo Jardim, and Ponte Alta do Bom Jesus, in the Tocantins State (North Brazil) (Figure 1).

The study area is within the Cerrado biome, which has vegetation constituted by a heterogeneous mosaic of forest, shrub, and grass-dominated formations (RIBEIRO; WALTER, 2008). The dominant climate class, according to the Köppen-Geiger classification, is the continental tropical (Aw),

with dry winter and rainy summer. The rainfall data from the Empresa Baiana de Desenvolvimento Agrícola (EBDA, in Portuguese), the state organization for agricultural development in Bahia, indicate an average annual rainfall of 1,053 mm in the city of Barreiras, Bahia State.

Figure 1 - Location of the study area in western Bahia.
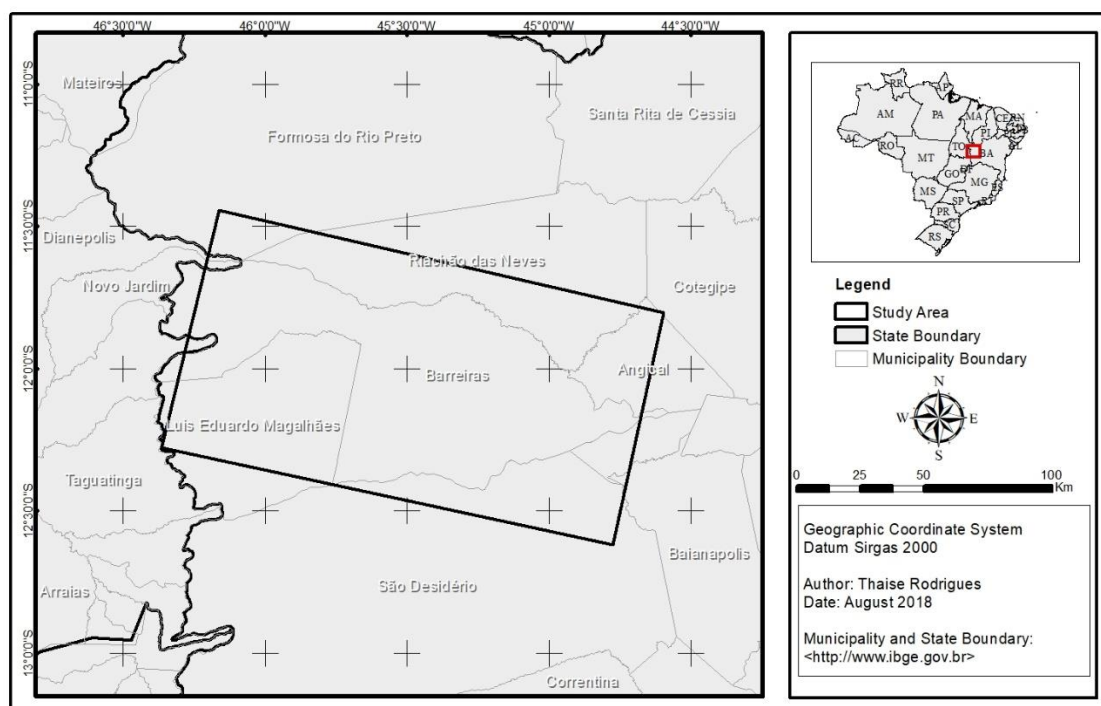
Source: Authors, 2018.

Materials

We used the Sentinel-1A satellite images from October 3, 2016, and October 22, 2017, and the Landsat-8 Operational Land Imager (OLI) satellite images from October 2, 2016, and February 23, March 27, April 28, May 30, July 17, September 19, and October 21, 2017. The Sentinel-1A (C-band) scenes were obtained from the Google Earth Engine (GEE) platform in the Interferometric Wide (IW) image acquisition mode, with two polarizations (VV and VH) and a pixel size of 20 m.

These images are available on the platform with some level of preprocessing, such as thermal noise removal, edge matching, radiometric calibration and orthorectification. In the orthorectification procedure, the data were converted to the backscatter coefficient (o°) using the 30-meter Shuttle Radar Topography Mission (SRTM) digital elevation model (DEM) or the Advanced Spaceborne Thermal Emission and Reflection Radiometer (ASTER) sensor for high latitudes (>60° or <-60°). The coefficients were then set at the 1st and 99th percentiles to preserve the dynamic range from the anomalous values and quantified to 16 bits. These steps followed the implementation in the Sentinel Application Platform (SNAP) toolbox, a Sentinel constellation image processing software freely available from the ESA (GEE, 2018). Landsat-8 images (bands 4, 5 and 6) were obtained from the US Geological Survey (USGS) website (earth explorer), with a spatial resolution of 30 m and were reprojected for the Southern Hemisphere, as the USGS provides images oriented for the Northern Hemisphere. This processing was performed in ArcGIS 10.1 software.

The land-use and land-cover (LULC) map of the Cerrado from 2013, which was produced by the TerraClass Cerrado project and developed under the coordination of the Brazilian Ministry of Environment (MMA, 2015) was also used. The land use-related classes of this project (annual cropland, perennial cropland, mining area, mosaic of land occupation, cultivated pasture, reforestation, bare soil, and urban area) were used as masks for the interpretation of the Sentinel-1A images. Because of the time gap between TerraClass Cerrado (mapping project based on Landsat-8 images from 2013) and this study, we updated the mask for 2016, based on the on-screen visual interpretation of the Landsat-8 images from October 2, 2016.

Methodological approach

With the support of the visual interpretation of the Landsat-8 scenes on the computer screen, the LULC mask, and the QGIS 2.14 software, the deforested areas in the study area were mapped for the following Sentinel-1A satellite overpasses: February 23, March 27, April 28, May 30, July 17, September 19, and October 21, 2017. A set of n deforestation polygon samples was then validated in the field. The minimum sample size was calculated as (LARSON; FARBER, 1999) (Eq. 1):

$$n = \frac{N.Z^2.p(1-p)}{(N-1).e^2 + Z^2.p(1-p)} \tag{1}$$

where n = number of the samples; N = size of the universe; Z = deviation from the accepted average value to achieve the desired confidence level; e = maximum allowable margin of error; and p = expected proportion. The field campaign was held on November 17-20, 2017.

The Sentinel-1A scenes were then rescaled from $\sigma°$ to digital numbers (*DNs*) (Eq. 2). A script was prepared for this procedure and was calculated as follows:

$$DN = 10^{\sigma°(dB)/10} \tag{2}$$

The scenes were then processed by the low-pass spatial filtering technique to reduce the speckle effect, a type of multiplicative and random noise that is inherent in all radar image acquisition processes. Filters should not only maintain approximately the average backscatter intensity of images but also reduce variance and preserve edges and texture (DONG et al., 2001). In this study, the refined Lee adaptive filter and Quegan & Yu filter were considered. The former selects neighboring pixels with similar scattering characteristics (LEE et al., 2006), while the latter is a linear filter, making it

suitable for relatively long time series of images (QUEGAN; YU, 2001). Examples of the application of these two filters can be found in Vasile et al. (2010) and Bejima et al. (2014) (refined Lee filter) and in Engdahl and Hyyppä (2003) and Bouvet et al. (2009) (Quegan & Yu filter).

The deforestation polygons detected through the Landsat-8 images were inserted into the GEE platform so that the average DNs for each deforestation polygon could be extracted. We then calculated the ratios between the 2017 (T1) and 2016 (T0) images for both VV and VH polarizations and both the unfiltered images and those processed by refined Lee and Quegan & Yu filters. These products returned images that highlighted the changes in areas where the backscatter shifted in intensity. This method corresponded to the basic operation of the change detection tool available in the SNAP change detection software.

Then, the images were reconverted to o° (Eq. 3) to allow the extraction of the backscatter values from T0 and T1 for the unfiltered VV and VH polarizations and processed with the two filters mentioned above. The T1/T0 ratio values and T0 and T1 backscatter values were analyzed through boxplots to establish the three deforestation thresholds. The updated land use-related mask for 2016 was one of the input parameters of the script so that detection was performed only in areas with natural vegetation cover; the calculation is written as follows:

$$\sigma°(dB) = 10\log(DN) \tag{3}$$

The three thresholds corresponded to the upper, middle, and lower limits of the minimum and maximum *DNs* shown in the boxplots. These deforestation thresholds were inserted in the script developed in the GEE platform to export a raster file converted into TIFF format containing these thresholds. The file was then converted to the vector format for area estimation of the deforestation polygons and exclusion of polygons smaller

than 2 hectares. The polygons detected according to the selected thresholds were validated through comparison with the deforestation data derived from the Landsat-8 images in terms of the errors of omission and commission.

RESULTS AND DISCUSSION

The Landsat-8 OLI image interpretation produced a set of 195 deforestation polygons. Thirty-two polygons were located in the municipality of Angical, 82 in Barreiras, 7 in Catolândia, 28 in Luís Eduardo Magalhães, 24 in Riachão das Neves, and 22 in São Desidério. Figure 2 shows an example of a deforested area in the municipality of Barreiras in the RGB color composite of the bands 6, 5, and 4 of the Landsat-8 satellite and the corresponding Sentinel-1A images in the VV and VH polarizations.

Figure 2 - RGB color composites of bands 6, 5 and 4 of the Landsat-8 satellite from October 2, 2016, and October 21, 2017,(before and after deforestation) in (a) and (d) and the corresponding images from the Sentinel-1A satellite obtained on October 3, 2016, and November 10, 2017, on VV polarization in (b) and (e) and VH polarization in (c) and (f).
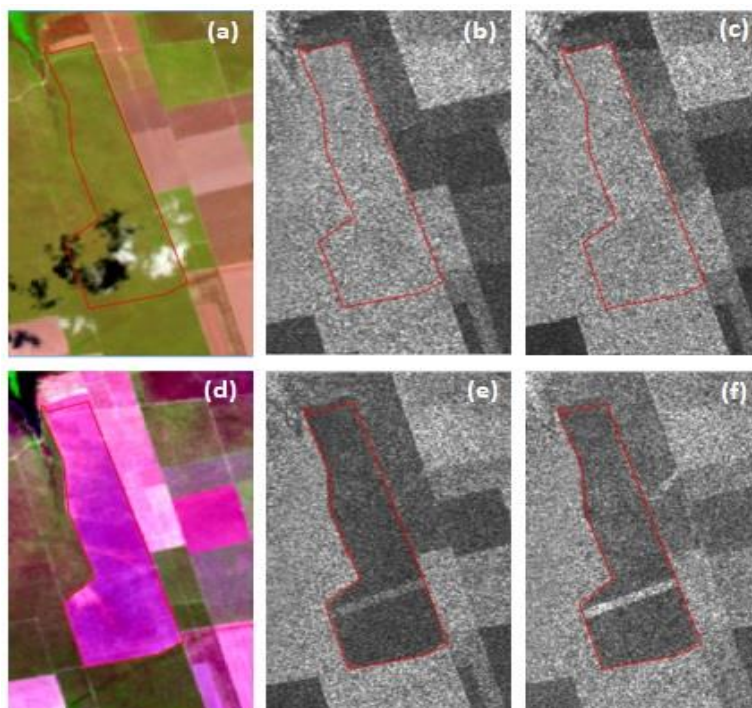
Source: Authors, 2018.

We noted that the deforested area appeared in dark gray tones in the Sentinel-1A images for both polarizations. This was because the removal of the trees and bushes eliminated a large number of the individual scatterers that contributed to the backscattering processes of the radar pulses emitted by the imaging sensors. As a result, most deforested areas in the Cerrado appeared with dark gray tones. Exceptions to this rule occurred when there was rainfall soon before the radar satellite overpass because the increase in soil moisture increased the backscattering of incident radiation (MENESES; ALMEIDA, 2012) or when the satellite overpass was soon after the deforestation event, so that the trunks and branches still remained on the ground, increasing the roughness of the terrain (ALMEIDA FILHO et al., 2007).

Considering the set of 195 deforestation polygons, the 10% maximum margin of error and the 90% confidence level, the minimum number of validation samples would be 48, according to Eq. 1. In this study, we surveyed 49 sites in the field. A total of 36 sites presented trunks and branches on the ground (scattered or mulched), selective logging for timber exploration, fire scars, and bare soils (Figure 3).

In most polygons with deforestation that occurred between July and October 2017, according to the Landsat-8 image interpretation, we found branches and trunks on the terrain surface that were either burned or unburned. Dead vegetation was also found in most of the smaller deforestation polygons and on relatively old deforestation areas, indicating that terrain clearing may occur mainly on larger farms because of their better economic conditions.

Figure 3 - Different aspects of the deforested areas found in the field: recent deforestation, with trunks and branches left on the terrain (a); selective logging for timber exploration (b); fire scars in a previously deforested area (c); and bare soils prepared for crop or pasture plantation (d).

Large deforested areas were located mainly in the municipalities of Barreiras and Luís Eduardo Magalhães, while the small deforested areas were mostly found in the municipalities of Riachão das Neves and Angical (Figure 4).
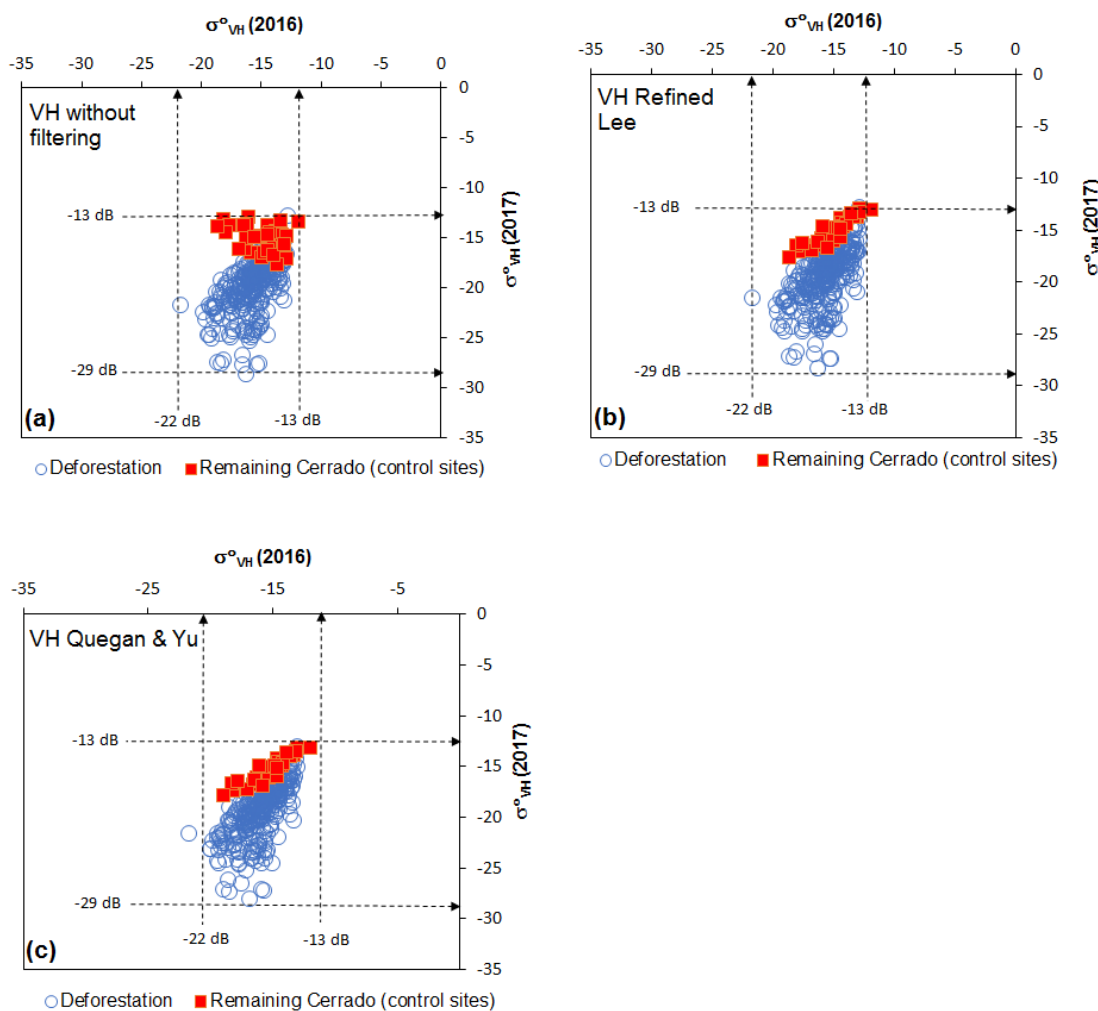
Figure 4 - Deforestation polygons identified through the visual interpretation of Landsat-8 images from 2016 and 2017.
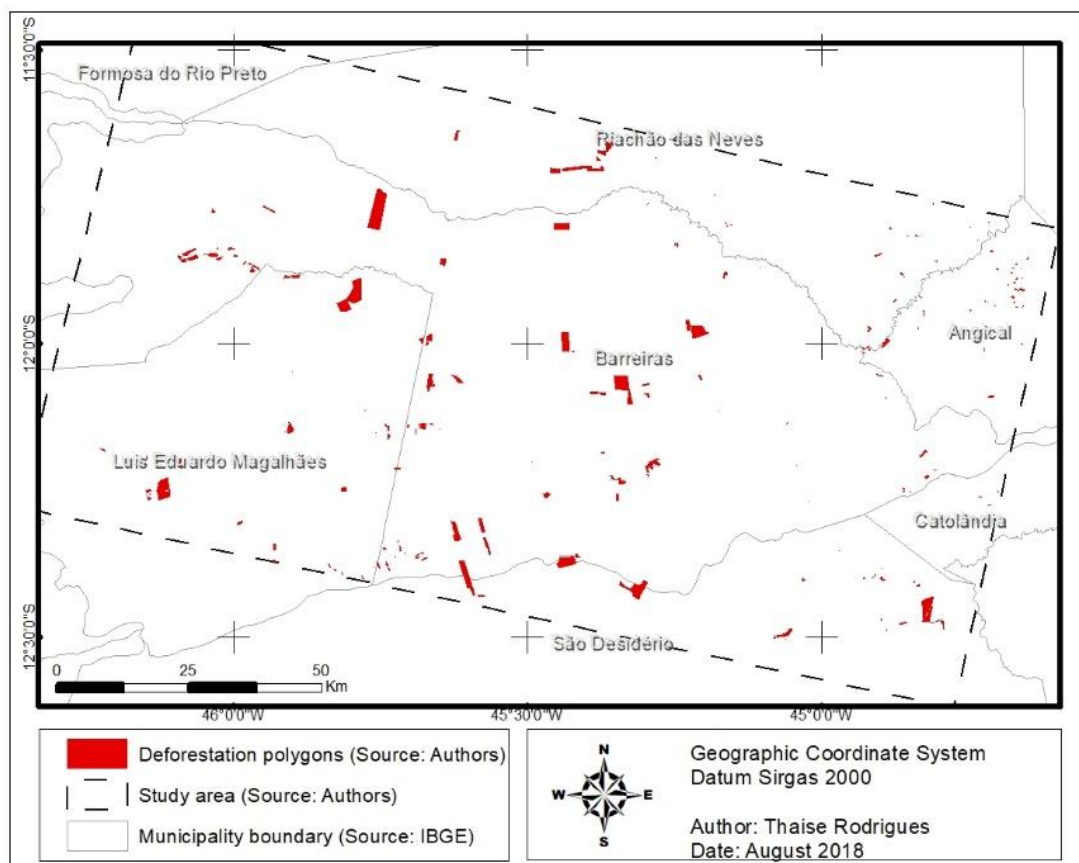
Source: Authors, 2018.

Figure 5 shows the scatterplots between the σ° values in the VV polarization, which were extracted from the deforestation polygons and the remaining Cerrado polygons (control sites) identified in the Landsat-8 images, with and without spatial filtering. Almost all polygons showed decreased σ° values after the deforestation event, from roughly -14 dB to -7 dB (natural) to -20 dB to -8 dB (deforested). The application of the Lee and Quegan & Yu filters apparently did not show significant changes in relation to backscattering values without spatial filtering.

Figure 5 - Relationship between the backscatter coefficients (dB) from the deforestation polygons identified in the Landsat-8 images and the corresponding natural areas (control sites) in 2016 and 2017 in the VV polarization without spatial filtering (a), with application of the refined Lee filter (b), and with application of the Quegan & Yu filter (c).

Source: Authors, 2018.

Figure 6 shows the relationships between $\sigma°$ values in the VH polarization, extracted from the deforestation and remaining Cerrado (control sites) polygons identified in the Landsat-8 images, with and without spatial filtering. The decrease in the $\sigma°$ values after the deforestation event were again notable, ranging from -22 dB to -13 dB (natural) to -29 dB to -13 dB (deforested). Enhancements through the Lee and Quegan & Yu filters also showed no noticeable changes to these relationships.

Figure 6 - Relationship between the backscatter coefficients (dB) from the deforestation polygons identified in the Landsat-8 images and the corresponding natural areas (control sites) in 2016 and 2017 in VH polarization without spatial filtering (a), with application of the refined Lee filter (b), and with application of the Quegan & Yu filter (c).
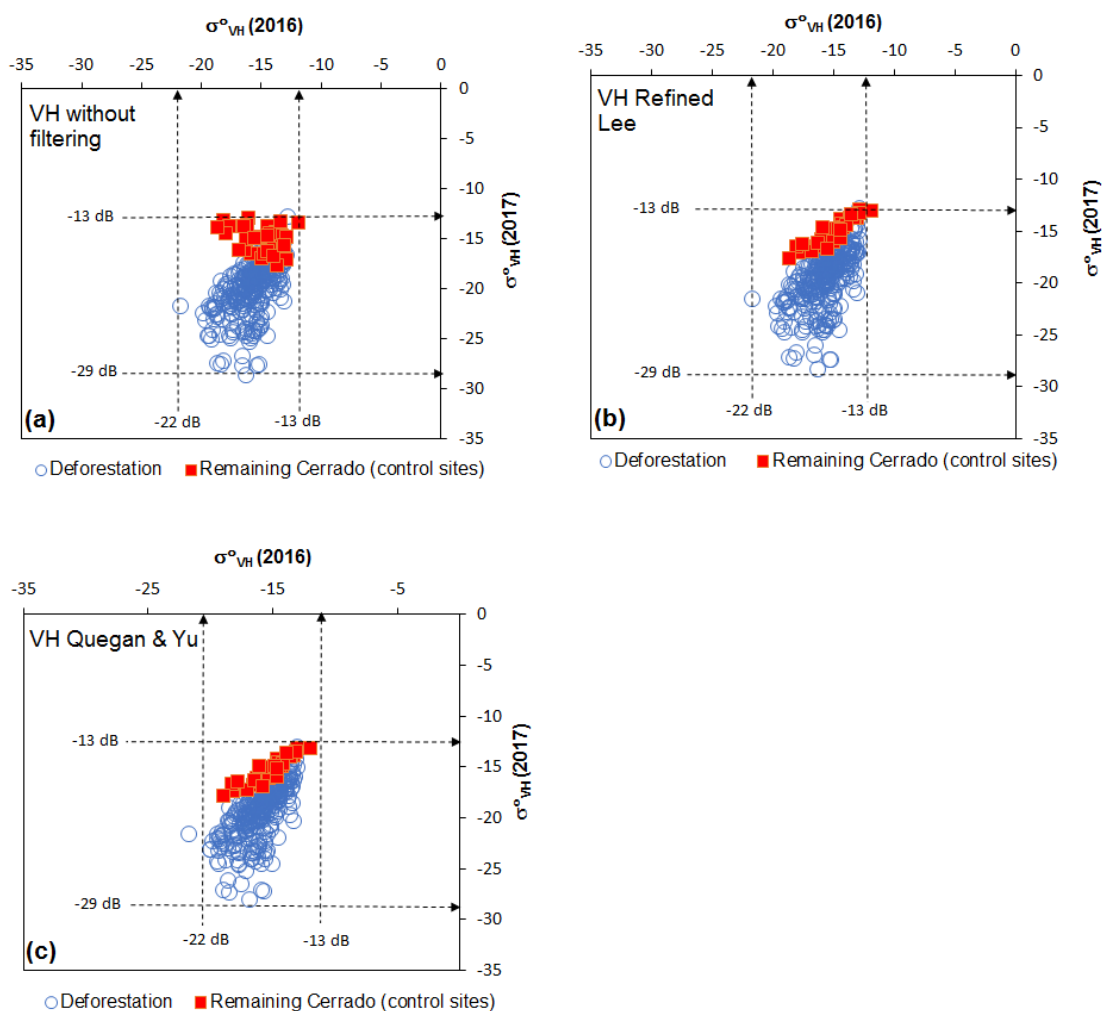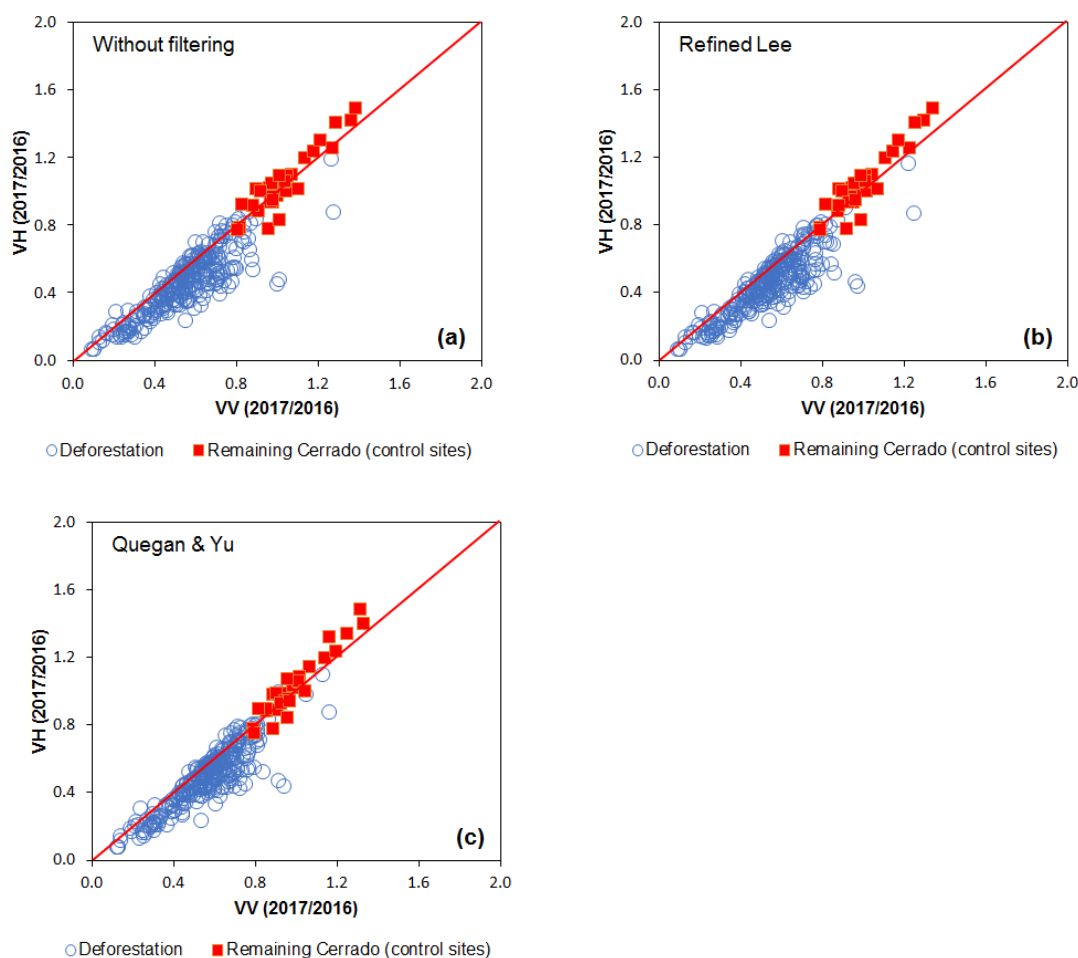

Source: Authors, 2018.

Figure 7 showed the relationships between the 2017/2016 ratio obtained for the VV and VH polarizations relative to the deforestation and Cerrado natural vegetation (control sites) polygons identified in Landsat-8 images, with and without spatial filtering. There was a clear separation between the deforested and natural vegetation polygons in both polarizations, with or without the use of spatial filters. Therefore, the 2017/2016 ratio

technique considered in this study demonstrated a high potential to identify deforested areas based on Sentinel-1A images.

Figure 7 - Relationship between the digital numbers obtained from the 2017/2016 ratio in the VV and VH polarizations for the deforestation and the corresponding Cerrado natural vegetation (control sites) polygons identified in the Landsat-8 images without spatial filtering (a), with application of the refined Lee filter (b), and with application of the Quegan & Yu filter (c).
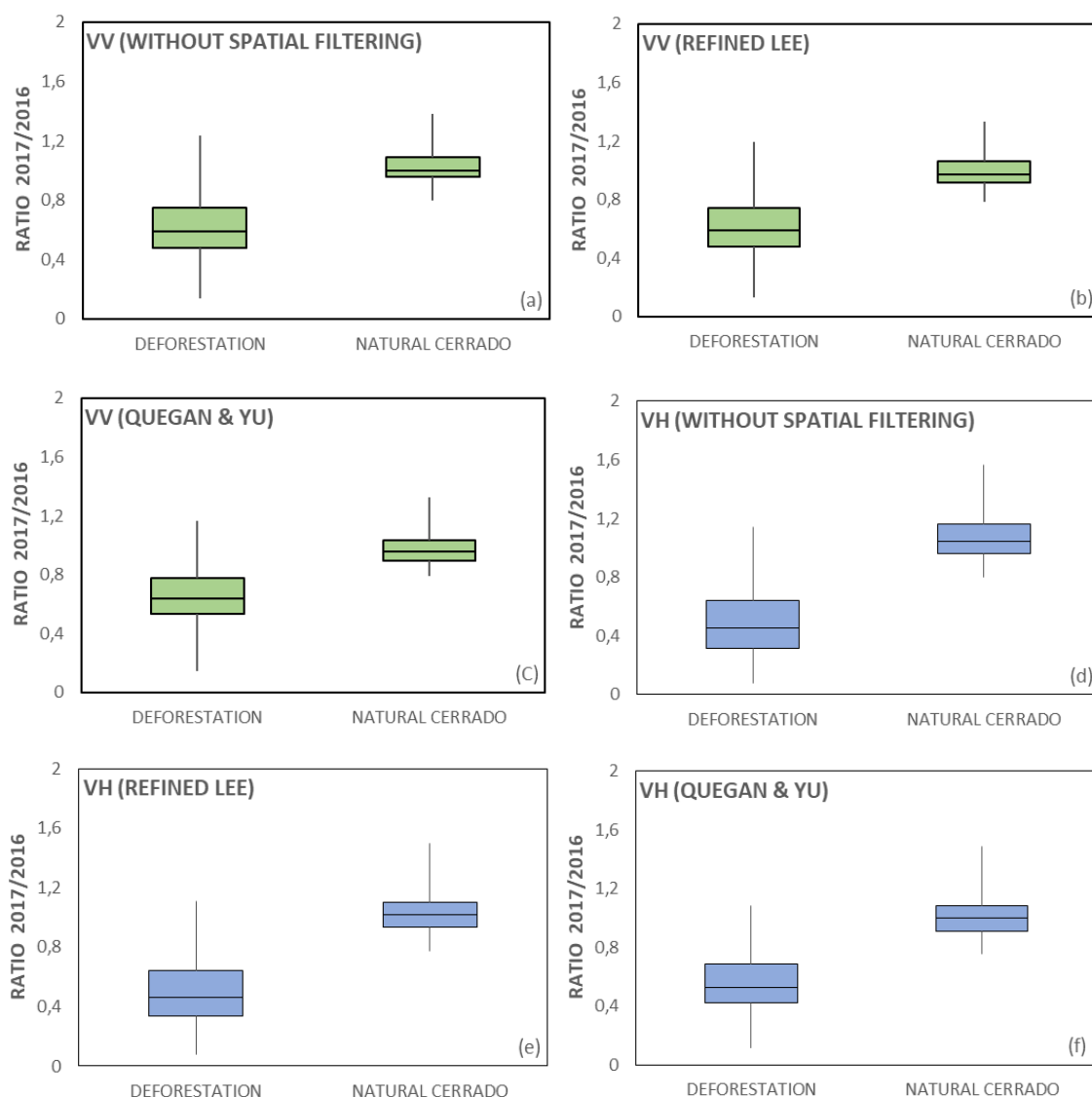

Source: Authors, 2018.

To better visualize the overall data distribution of the difference between the initial and final periods analyzed for the two classes, boxplots representing the quartiles of each dataset were prepared (Figure 8). Again, there was a clear separation between the two classes. In the VV polarization, there was an overlap of the maximum deforestation values with the minimum

values of the unchanged areas between 0.8 and 0.9; however, when considering the average of 0.6 for this dataset, it was possible to consider a threshold below 0.8.

Figure 8 - VV and VH polarization boxplots representing the distribution in quartiles of the 2017/2016 ratio data of deforestation and natural Cerrado (control sites), without spatial filtering [(a) and (d)], with application of refined Lee filter [(b) and (d)] and with application of the Quegan & Yu filter [(c) and (f)].

Source: Authors, 2018.

In the VH polarization, it was observed that the 2017/2016 ratio values were slightly lower; however, as in the VV polarization, there was a clear separation between the deforestation classes and the natural area classes. Most of the data for the deforestation polygons, until the 3rd quartile, were below 0.8. For the natural areas, the data above the 1st quartile were higher than 0.9. Between 0.8 and 0.9, there was also an overlap of the maximum deforestation values with the minimum values of natural vegetation covered areas. However, when considering that the average was 0.5 for this dataset, it was possible to consider a threshold below 0.8 for this polarization.

For each polarization, three thresholds were selected for the detection of deforestation in the study area: 0.6, 0.7, and 0.8 for VV polarization; and 0.6, 0.7, and 0.76 for the VH polarization. The proposed maximum thresholds had values above the averages presented to reduce the potential omission errors. After applying the thresholds to the Sentinel-1A data, the automatically detected polygons were compared with the previous deforestation polygons detected in the Landsat-8 images.

During the validation process, it was observed that the areas with fire scars were interpreted as deforestation. Therefore, we analyzed whether there was any difference between the backscattering coefficients from deforestation and those from fire scars. We concluded that there was no separation between the two classes, regardless of the polarization or filters. Thus, the polygons that were classified as burn scars were not considered in the accuracy analysis.

The deforestation data generated in the GEE platform using the VV polarization presented different results for the three thresholds (Table 1). The lower the threshold was, the higher the accuracy and omission error values were. The best result was obtained for the 0.60 threshold and for the refined Lee filter; however, there was no significant improvement in relation to the 0.70 threshold. The accuracy values for the VV polarization were generally lower than those for the VH polarization (Table 2). Only for the 0.70 and 0.60

thresholds in the Quegan & Yu filtered images were the accuracy values higher. On the other hand, there was also an increase in the omission error. In the VH polarization, lower thresholds resulted in higher accuracy but also in higher omission error (same pattern observed for the VV polarization). The best result was also obtained for the 0.60 threshold and refined Lee filtered images, which did not have a considerable increase in the 0.70 threshold omission error.

Table 1. Overall accuracy and omission error calculated for the Sentinel-1A automatic detection data and validated based on the deforestation data obtained from the Landsat-8 images for the VV polarization, with and without spatial filtering.

Treatment	Accuracy/Error	Thresholds		
	(%)	0.80	0.70	0.60
Without filtering	Overall accuracy	91.80	91.80	91.80
	Omission error	52.88	52.88	52.88
Refined Lee filtering	Overall accuracy	77.53	87.96	92.77
	Omission error	53.22	53.22	54.24
Quegan & Yu filtering	Overall accuracy	15.22	66.67	86.43
	Omission error	21.69	35.93	54.24

Source: Authors, 2018.

Table 2. The overall accuracy and omission error calculated for the Sentinel-1A automatic detection data validated based on the deforestation data obtained from the Landsat-8 images for the VH polarization, with and without spatial filtering.

Treatment	Accuracy/Error	Thresholds		
	(%)	0.76	0.70	0.60
Without filtering	Overall accuracy	93.08	93.08	93.08
	Omission error	38.64	38.64	38.64
Refined Lee filtering	Overall accuracy	91.26	91.26	95.02
	Omission error	38.21	38.31	38.64
Quegan & Yu filtering	Overall accuracy	38.31	56.14	86.21
	Omission error	18.98	22.71	37.97

Source: Authors, 2018.

According to Almeida Filho et al. (2007, 2010) and Aboud Neta et al. (2010), the omission errors occurred as a result of the vegetation debris left

in the soil, in cases of recent deforestation, as these materials tended to increase the backscatter in the radar images. However, when analyzing the cases of omission by the period of occurrence in Landsat-8 images, it was observed that these polygons did not have a pattern related to the date of deforestation. This fact, which was typical of the deforestation in the Amazon, cannot be applied indiscriminately to the deforestation in the Cerrado since the time of the deforestation processes and the burning and clearing activities after deforestation in the Cerrado depend on the landowner's financial resources.

Concluding Remarks

Based on the obtained results, we can conclude that the Sentinel-1A satellite radar images can be used to detect the changes in the natural vegetation cover of the Cerrado. In other words, the images from this satellite can be used to support inspection and management of illegal deforestation in this biome. In addition, the results obtained by this study allowed the following conclusions:

1) The images processed with the refined Lee filter performed well in detecting the changes in the vegetation cover and were more effective in comparison with the unfiltered images or those processed with the Quegan & Yu filter;

2) The VH polarization, in comparison with the VV polarization, showed superior results in detecting deforestation;

3) The Google Earth Engine platform proved to be effective for the selection, preprocessing, and processing of the radar data;

4) The main difficulty encountered in this study was the use of a relatively new image processing platform that required prior knowledge of the programming language to execute scripts and algorithms;

5) There is a lack of studies that involve the use of radar images for monitoring of the Cerrado, which makes it difficult to compare the results of this study with other data from the literature;

6) Continuation of this study is recommended through investigation, for example, of the potential of the integrated use of both optical and radar images from the Sentinel-1 and Sentinel-2 satellites, both of which were freely available on the internet, to improve the accuracy of the identification of areas with changes in Cerrado vegetation.

References

ABOUD NETA, S. R.; FREITAS, C. C.; DUTRA, L. V. Uso de imagens ALOS/PALSAR multipolarizadas para detecção de incremento de desflorestamento na Amazônia. **Revista Brasileira de Cartografia**, v. 62, n. 2, p. 417-431, 2013.

ALMEIDA FILHO, R.; ROSENQVIST, A.; SHIMABUKURO, Y. E.; SILVA-GOMEZ, R. Detecting deforestation with multitemporal L-band SAR imagery: a case study in western Brazilian Amazônia. **International Journal of Remote Sensing**, v. 28, n. 6, p. 1383-1390, 2007. https://doi.org/10.1080/01431160600754591

ALMEIDA FILHO, R.; SHIMABUKURO, Y. E. Detecting areas disturbed by gold mining activities through JERS-1 SAR images, Roraima State, Brazilian Amazon. **International Journal of Remote Sensing**, v. 21, n. 17, p. 3357-3362, 2010. https://doi.org/10.1080/014311600750019967

BEJIMA, S. V.; COMBER, A.; LAMB, A. Random forest classification of salt marsh vegetation habitats using quad-polarimetric airborne SAR, elevation and optical RS data. **Remote Sensing of Environment**, v. 149, p. 118-129, 2014. https://doi.org/10.1016/j.rse.2014.04.010

BOUVET, A.; LE TOAN, T.; LAM-DAO, N. Monitoring of the rice cropping system in the Mekong delta using ENVISAT/ASAR dual polarization data. **IEEE Transactions on Geoscience and Remote Sensing**, v., 47, n. 2, p. 517-526, 2009. https://doi.org/10.1109/TGRS.2008.2007963

BRANNSTROM, C.; JEPSON, W.; FILIPPI, A. M.; REDO, D.; XU, Z.; GANESH, S. Land change in the Brazilian savanna (Cerrado), 1986-2002: comparative analysis and implications for land-use policy. **Land Use Policy**, v. 25, n. 4, p. 579-595, 2008. https://doi.org/10.1016/j.landusepol.2007.11.008

CARNEIRO FILHO, A.; COSTA, K. **A expansão da soja no Cerrado**. Caminhos para a ocupação territorial, uso do solo e produção sustentável. São Paulo: Agroícone, 28 p., 2016.

DONG, Y.; MILNE, A. K.; FORSTER, B. C. Toward edge sharpening: a SAR speckle filtering algorithm. **IEEE Transactions on Geoscience and Remote Sensing**, v. 39, n. 4, p. 851-863, 2001. https://doi.org/10.1109/36.917910

ENGDAHL, M. E.; HYYPPÄ, J. M. Land-cover classification using multitemporal ERS-1/2 InSAR data. **IEEE Transactions on Geoscience and Remote Sensing**, v. 41, n. 7, p. 1620-1628, 2003. https://doi.org/10.1109/TGRS.2003.813271

ESA. European Space Agency. **Sentinel-1: User Handbook**, ESA Standard Document, 2013.

FERREIRA, N. M.; FERREIRA, L. G.; FERREIRA, N. C.; ROCHA, G. F.; NEMAYER, M. Desmatamentos no bioma Cerrado: uma análise temporal (2001-2005) com base nos dados

MODIS - MOD13Q1. In: Simpósio Brasileiro de Sensoriamento Remoto, 13., Florianópolis, SC. **Anais.** São José dos Campos: INPE, p. 3877-3883, 2007.

FLORES, P. M.; GUIMARÃES, R. F.; CARVALHO JÚNIOR, O. A.; GOMES, R. A. T. Análise multitemporal da expansão agrícola no município de Barreiras – Bahia (1988-2008). **Campo-Território**, v. 7, n. 14, p. 1-19, 2012.

GEE. Google Earth Engine. **Sentinel-1 algorithms**. 2018. Disponível em: <https://developers.google.com/earth-engine/sentinel1>. Acesso em: 17 de agosto de 2018.

LARSON, R.; FABER, B. **Elementary Statistics. Picturing the World**. (tradução de Luciane Vianna), 5ª ed. São Paulo: Pearson Prentice Hall, 1999, 45 p.

LEE, J. S.; GRUNES, M. R.; SCHULER, D. L.; POTTIER, E.; FERRO-FAMIL, L. Scattering-model-based speckle filtering of polarimetric SAR data. **IEEE Transactions on Geoscience and Remote Sensing**, v. 44, n. 1, p. 176-187, 2006. https://doi.org/10.1109/TGRS.2005.859338

MENESES, P. R.; ALMEIDA, T. **Introdução ao Processamento de Imagens de Sensoriamento Remoto**. 1ª ed. Brasília: CNPq, 2012.

MENKE, A. B.; CARVALHO JÚNIOR, O. A.; GOMES, R. A. T.; MARTINS, E. S.; OLIVEIRA, S. N. Análise das mudanças do uso agrícola da terra a partir de dados de sensoriamento remoto multitemporal no município de Luís Eduardo Magalhães (BA – Brasil). **Sociedade & Natureza**, v. 21, n. 3, p. 315-326, 2009. http://dx.doi.org/10.1590/S1982-45132009000300007

MMA. Ministério do Meio Ambiente. **Mapeamento do uso e cobertura do Cerrado: Projeto Terra Class Cerrado 2013**. Brasília: MMA, 67 p., 2015.

MMA. Ministério do Meio ambiente. **O bioma Cerrado**. Disponível em: <http://www.mma.gov.br/biomas/cerrado>. Acesso em: 21 de janeiro de 2018.

MONDARDO M. L. A "territorialização" do agronegócio globalizado em Barreiras – BA: migraçao sulista, reestruturação produtiva e contradições sócio-territoriais. **Revista Nera**, v. 13, n. 17, p.112-130, 2010.

QUEGAN, S.; YU, J. J. Filtering of multichannel SAR images. **IEEE Transactions on Geoscience and Remote Sensing**, v. 39, n. 11, p. 2317-2379, 2011. https://doi.org/10.1109/36.964973

RADA, N. Assessing Brazil's Cerrado agricultural miracle. **Food Policy**, v. 38, p. 146-155, 2013. https://doi.org/10.1016/j.foodpol.2012.11.002

RIBEIRO, J. F.; WALTER, B. M. T. As principais ftofsionomias do Cerrado. In: SANO, S. M.; ALMEIDA, S. P.; RIBEIRO, J. F. (eds.). **Cerrado: Ecologia e Flora**, Planaltina: Embrapa Cerrados, p. 151-199, 2008.

SANO, E. E.; ROSA, R.; BRITO, J. L.; FERREIRA, L. G. Land cover mapping of the tropical savanna region in Brazil. **Environmental Monitoring & Assessment**, v. 166, n. 1-4, p. 113-124, 2010. https://doi.org/10.1007/s10661-009-0988-4

SANTOS, M. A.; BARBIERI, A. F.; CARVALHO, J. A. M.; MACHADO, C. J. **O Cerrado Brasileiro.** Notas para Estudo. Belo Horizonte: UFMG/CEDEPLAR, n. 387, 15 p., 2010.

SILVA, J. M. C.; BATES, H. M. Biogeographic patterns and conservation in the South American Cerrado: a tropical savanna hotspot. **BioScience**, v. 52, n. 3, p. 225-234, 2002. https://doi.org/10.1641/0006-3568(2002)052[0225:BPACIT]2.0.CO;2

TORRES, R.; SNOEIJ, P.; GEUDTNER, D.; BIBBY, D.; DAVIDSON, M. et al. GMES Sentinel-1 mission. **Remote Sensing of Environment**, v. 120, p. 9-24, 2012.

VASILE, G.; OVARLEZ, J. P.; PASCAL, F.; TISON, C. Coherency matrix estimation of heterogeneous clutter in high-resolution polarimetric SAR images. **IEEE Transactions on Geoscience and Remote Sensing**, v. 48, n. 4, p. 1809-1826, 2010. https://doi.org/10.1109/TGRS.2009.2035496